materials

MDPI

Article

The Effect of d^{10} Precious Elements on Structural, Magnetic and Elastic Properties of MnPt Alloy: A First-Principles Study

Ramogohlo Diale [1,*], Phuti Ngoepe [2], Hasani Chauke [2], Joseph Moema [1] and Maje Phasha [1]

[1] Advanced Materials Division, Mintek, Private Bag X 3015, Randburg 2125, South Africa; josephm@mintek.co.za (J.M.); majep@mintek.co.za (M.P.)
[2] Materials Modelling Centre, University of Limpopo, Private Bag X 1106, Sovenga 0727, South Africa; phuti.ngoepe@ul.ac.za (P.N.); hasani.chauke@ul.ac.za (H.C.)
* Correspondence: ram@mintek.co.za

Abstract: MnPt's exceptional stability and extremely high Néel temperature have generated a lot of interest in data storage applications. Previously, it was reported experimentally that the MnPt alloy shows ferromagnetic (FM) behavior at room temperature. In this study, the effects of partial substitution of Pt with Pd, Au, and Ag on magnetic properties is investigated using density functional theory. The stability of $Mn_{50}Pt_{50-x}M_x$ (M = Pd, Au, Ag, x = 6.25, 12.5, 18.75) alloys was assessed by determining their thermodynamic, magnetic, and mechanical properties. The calculated lattice constants of $Mn_{50}Pt_{50}$ agree well with available theoretical results. The $Mn_{50}Pt_{50-x}M_x$ alloys' formability was assessed by measuring the thermodynamic stability using the heat of formation. It was found that B2 $Mn_{50}Pt_{50-x}Pd_x$ alloys ($0 \leq x \leq 18.75$) are thermodynamically stable due to the negative heat of formation close to that of a pristine MnPt alloy. Based on the elasticity results, the B2 $Mn_{50}Pt_{50-x}Pd_x$ is most likely to undergo martensitic transformation for the entire considered composition range. From the calculated values of the Poisson's ratio, it is shown that an increase in Pd, Ag, and Au effectively improves the ductility of the B2 $Mn_{50}Pt_{50-x}M_x$ compounds. It was revealed that ferromagnetism is maintained with Pd addition but significantly reduced in the case of Au and Ag. Thus, this work showed that density functional theory can be exploited to propose new possible compositions for future magnets in spintronic applications.

Keywords: $Mn_{50}Pt_{50-x}M_x$ (M = Pd; Au; Ag); magnetic properties; elastic properties; density functional theory

Citation: Diale, R.; Ngoepe, P.; Chauke, H.; Moema, J.; Phasha, M. The Effect of d^{10} Precious Elements on Structural, Magnetic and Elastic Properties of MnPt Alloy: A First-Principles Study. *Materials* **2024**, *17*, 541. https://doi.org/10.3390/ma17030541

Academic Editors: Bryan M. Wong and Shaohong Liu

Received: 26 November 2023
Revised: 17 January 2024
Accepted: 19 January 2024
Published: 23 January 2024

1. Introduction

Manganese (Mn) has received considerable attention in the past few years due to its low cost as a result of its abundance in the earth's crust as well as its fascinating magnetic properties, which emerge when the separation distance between its atoms is increased by the presence of elements with either larger atomic radius or higher melting point to form an ordered intermetallic phase [1]. As a result of their half-filled 3d orbitals, most Mn-based intermetallic compounds formed at near-equiatomic composition with elements belonging to groups 9 and 10 of the periodic table reveal a typical antiferromagnetic (AFM) characteristic [2,3]. It is this characteristic and other properties, such as high stability of antiferromagnetism as well as very high Néel temperature (T_N), that have aroused significant interest in AFM materials such as NiMn, IrMn, PdMn, RhMn and MnPt for their potential practical applications in the microelectronics industry. In contrast to conventional spintronic devices which use FM as the active element, the anti-ferromagnet spintronics use the AFM as the active element to store, read or write data much faster. One of the major attractive points of AFM materials is their insensitiveness to parasitic electromagnetic and magnetic interference [4]. However, the magnetization of AFMs is very difficult to manipulate [5]. As deployed successfully in giant magnetoresistance (GMR) sensors, the

best of both is achieved by coupling the AFM to an FM. This vital exchange biasing between AFM and ferromagnetic (FM) layers in thin films results in the pinning effect by the AFM on an FM in magnetoresistance sensor and spin-valve heads [6]. The chief goal in this research and development effort is to achieve energy-efficient data storage by, in principle, finding a substitute for hard disk drives (HDD) and highly volatile dynamic random-access memory (DRAM) with a better multi-tasking performance at lower power consumption [7].

Among the above AFM material contenders, MnPt is the only one that exhibits the ferromagnetic exchange interactions characterized by out-of-plane equilibrium spin texture [2,4]. Due to its high ferromagnetic stability, it possesses excellent properties such as large exchange coupling fields and high blocking temperatures [8–10]. The equiatomic MnPt consists of the ordered paramagnetic cubic structure of type B2 (Pm-3m), which is transformed to a tetragonal structure of type $L1_0$ (CuAu-I) at 970 K. AFM coupling between adjacent Mn atoms in the (100) plane at a distance and ferromagnetic coupling between adjacent Mn atoms in the [001] direction account for the AFM ordering in MnPt experiments [11]. On the other hand, although it is difficult to process, the formation of FM phases is scarcely reported to occur in the MnPt samples, resulting in disordered and partially ordered Mn atoms [8]. A lot of interest has been taken in MnPt alloys lately since the type of magnetic interaction can be studied based on degree of order, atom separation, and even environmental factors [12]. Moreover, since it is known that the magnetic moment of Mn is higher than that of ferromagnetic metals such as iron (Fe), cobalt (Co) and nickel (Ni), research on how this FM aspect can be exploited for technological benefits is necessary.

In addition to magnetic recording and spintronic applications, MnPt permalloys can also be used as FM active elements instead of AFM active elements in magnetic random-access memory (MRAM). Magnetic susceptibility and electrical resistivity of MnPt alloys have been reported at 1220 K [13,14]. This viewpoint also brings about the possibility of having an exchange bias between FM and AFM comprised of only MnPt alloys. However, the processing of the binary MnPt alloys remains a huge obstacle to this possibility. The structural, electronic, and magnetic properties of the ordered binary $L1_0$ FePt, MnPt, and $CrPt_3$ alloys were determined using the density functional theory (DFT) approach in a previous study [15]. It was found that $L1_0$ MnPt exhibits magnetocrystalline anisotropy energy (MAE) values of 0.46 meV/f.u (1.3×10^7 erg/cm^3). It has been found that the smaller MAE value of $L1_0$ MnPt can be attributed to weak hybridization between Mn-3d and Pt-5d states. Due to its capability to provide insightful information on materials behavior, this theoretical platform can also be used to search for suitable alloying elements that can stabilize the FM MnPt, thus easing the processing challenges.

In this regard, the current authors have previously reported the effect of antiferromagnetic (Cr) and ferromagnetic (Fe) elements on MnPt alloy using the DFT-based first-principles calculations [16]. It was discovered that the inclusion of Fe causes the magnetic moment to fall below that of $Pt_{50}Mn_{50}$, while the magnetism is enhanced when c/a is 1.10 for $Pt_{50}Mn_{43.75}Cr_{6.25}$. The $L1_0$ phase was preferred over the B2 phase by both Fe and Cr on the Mn-site, as demonstrated by the thermodynamic and mechanical stability. Furthermore, in another study, we investigated the effect of ferromagnetic element (Co) on the magnetic properties of $Mn_{50}Pt_{50}$ alloy using the same theoretical approach [17]. The findings indicated that because of the negative heats of formation, the addition of Co favored $L1_0$ over the B2 phase. The study revealed that the addition of Co on both B2 and $L1_0$ $Mn_{50}Pt_{50}$ results in improved magnetic strength and mechanical stability on the Pt-site. Based on the findings above, it is clear that magnetic strength and mechanical stability can be improved on the Pt-site as compared to the Mn-site. While most first-principles studies have focused on AFM MnPt, the current focus is on an attempt to stabilize FM MnPt-X in the B2 phase.

In the current work, the ab initio DFT approach was used to investigate the effect of the d^{10} elements (Pd, Au, Ag) on the structural, thermodynamic, magnetic and elastic properties of $Mn_{50}Pt_{50-x}M_x$ ternary compositions. The choice of these alloying elements was based on our interest in studying the effect of introducing elements with larger atomic

radii on the Pt-site. The rest of this paper is organized as follows. The theoretical method of calculation is provided in Section 2, and the results such as the heat of formation, magnetic moments, elastic constants and moduli are discussed in Section 3. Lastly, a conclusion is provided in Section 4.

2. Computational Method

In this paper, calculations on structural, magnetic, and elastic properties were performed using density functional theory (DFT) employing the Vienna ab initio simulation package (VASP) [18,19]. The Projector Augmented Wave (PAW) pseudopotentials were used to describe electron-ion interactions. The spin-polarized generalized gradient approximation (GGA) [20], parameterized by Perdew–Burke–Ernzerhof (PBE) [21], was used to account for the exchange-correlation functional. A spin polarization was included in our calculations. Regarding the number of k-points and the plane-waves basis set size, the convergence of the total energies was examined. The real ionic and valence electron interaction was described by ultra-soft pseudopotential based on the first-principles calculations. The total energy of the structures was converged using a 500 eV plane wave cutoff energy. We carried out sets of calculations of B2 $Mn_{50}Pt_{50-x}M_x$ alloys ($0 \leq x \leq 18.75$) with a mesh grid of $14 \times 14 \times 14$ to converge the total energy of the structures, according to Monkhorst and Pack [22]. For the force theorem calculation alone, the spin-orbit coupling was taken into consideration. A $2 \times 2 \times 2$ supercell was used to perform the calculations. Using a substitutional search tool integrated into MedeA, Pt was replaced with Pd, Au, and Ag to produce the most stable compositions, which included 6.25, 12.50, and 18.75 at. % at the appropriate symmetry. The setting of "accurate" was applied throughout the calculation procedure to reduce errors and avoid wrap-arounds. Then, every structure was completely relaxed. Following the relaxed atomic positions, the total energy was minimized (i.e., as small as 10^{-6} eV) and the Hellmann–Feynman forces. In the unit cell of every electronic structure relaxation that was carried out, these forces were as small as 0.0003 eV/Å at convergence. A strain of 0.005 was used to calculate elastic constants for all structures. Using the Voigt approximation, the bulk modulus, shear modulus, elastic modulus, and Poisson ratio were consequently determined [23]. The paramagnetic and ferromagnetic B2 MnPt alloy phonon dispersion curves were assessed using the PHONON code [24] as implemented in Materials Design within the MedeA software platform, version 3.6. Each and every calculation was done at 0 K.

3. Results and Discussion

3.1. Structural and Magnetic Properties

In the MnPt alloy, the cubic B2 phase and the tetragonal $L1_0$ crystal structure exist at high and low temperatures, respectively. The high temperature phase (B2) belongs to space group Pm-3m, No: 221 with the following Wyckoff atomic positions: Mn located at 1a (0, 0, 0) and Pt at 1b (1/2, 1/2, 1/2). The low temperature phase ($L1_0$) belongs to space group P4/mmm, No: 123 with Wyckoff atomic position of Mn at 1a (0, 0, 0) and Pt at 1d (0, 1/2, 1/2).

The B2 MnPt alloy exists in two magnetic states at high temperatures, namely the paramagnetic (PM) and ferromagnetic (FM) phases. Both crystal structures consist of the same space group and Wyckoff atomic positions. Their main difference is the distance between atoms, i.e., from Mn to Pt and from Mn to Mn as well as from Pt to Pt. For example, FM MnPt has a distance of 2.70 Å from Mn1-Pt1, 3.12 Å from Mn1-Mn1 and 3.12 Å from Pt1-Pt1. In the case of PM, MnPt is 2.60 Å from Mn1-Pt1 and 3.00 Å from Mn1-Mn1, as well as 3.00 Å from Pt1-Pt1. The atomic arrangement of the two systems is the same as shown in Figure 1a,b with spins illustrated for the FM MnPt. The arrows indicate the relative directions of the Mn magnetic moment. The ferromagnetic behavior in Figure 1a is mainly a contribution of Mn atoms, while Pt atoms contribute a small amount of magnetic moment, due to the fact that Pt magnetic moments are significantly smaller than those of Mn. In the

case of PM MnPt, both Mn and Pt atoms show no contribution to the magnetic moment, which results in zero.

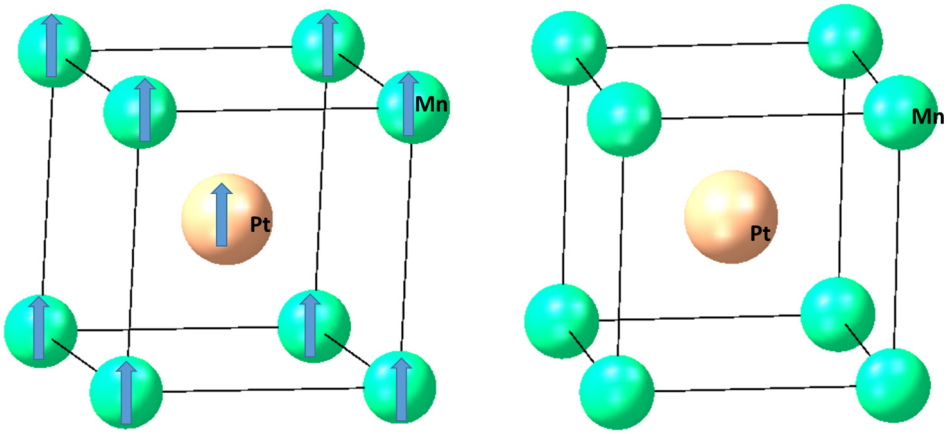

(**a**) (**b**)

Figure 1. Schematic picture of B2 MnPt in (**a**) ferromagnetic (FM) and (**b**) paramagnetic (PM) MnPt alloy.

Furthermore, the obtained lattice parameter of 3.00 Å for PM B2 is in excellent agreement with the theoretical value of 3.01 Å in the literature [25]. Due to the absence of reported data, the predicted lattice parameter of 3.12 Å for FM B2 could not be compared with any results. Since the focus of this work is on the FM B2 MnPt, the results presented below show how the introduction of precious elements (Pd, Ag, Au) affects the lattice parameters, heats of formation, magnetic moments, and elastic properties of the FM B2 MnPt alloy.

The computed lattice parameters of B2 $Mn_{50}Pt_{50-x}M_x$ alloys (M = Pd, Ag, Au) ($0 \leq x \leq 18.75$) are displayed in Figure 2a. Notably, the B2 $Mn_{50}Pt_{50-x}M_x$ lattice parameters show a slight decrease with Pd composition but an increase with M content for Ag and Au. This makes sense because Pt's atomic radius is marginally larger than Pd's (1.37 Å), but smaller than that of Ag (1.44 Å) and Au (1.44 Å). However, a significant increase in lattice parameter at 18.75 at. % Ag is noted. This behavior could be attributed to the higher coefficient of thermal expansion of Ag. In Figure 2b,c, the calculated heats of formation and the magnetic moments of the $Mn_{50}Pt_{50-x}M_x$ (M = Pd, Au, Ag) alloys along compositions are shown. The thermodynamic stability of B2 $Mn_{50}Pt_{50-x}M_x$ is discussed using the predicted heats of formation (ΔH_f) calculated using the following expression:

$$\Delta H_f = E_C - \sum_i x_i E_i, \quad (1)$$

where the total energy of the system is denoted by E_C and the total energy of its constituent elements is represented by E_i. The lowest negative value ($\Delta H_f < 0$) for the heat of formation is required for a structure to be considered stable, otherwise a positive value ($\Delta H_f > 0$) suggests instabilities.

The fact that Figure 2b shows that the B2 $Mn_{50}Pt_{50}$ alloy's heat of formation is negative suggests that there is a good chance that this compound will form.

Despite a slight increase, it is observed that B2 $Mn_{50}Pt_{50-x}Pd_x$ alloy compositions are thermodynamically feasible as indicated by the negative heats of formation for the considered composition range ($0 \leq x \leq 18.75$) as shown in Figure 2b. Furthermore, it is observed that the heat of formation increases with an increase in Ag and Au compositions as shown in Figure 2b. This suggests that the addition of Ag and Au reduces the thermodynamic stability, although the structures can be formed experimentally.

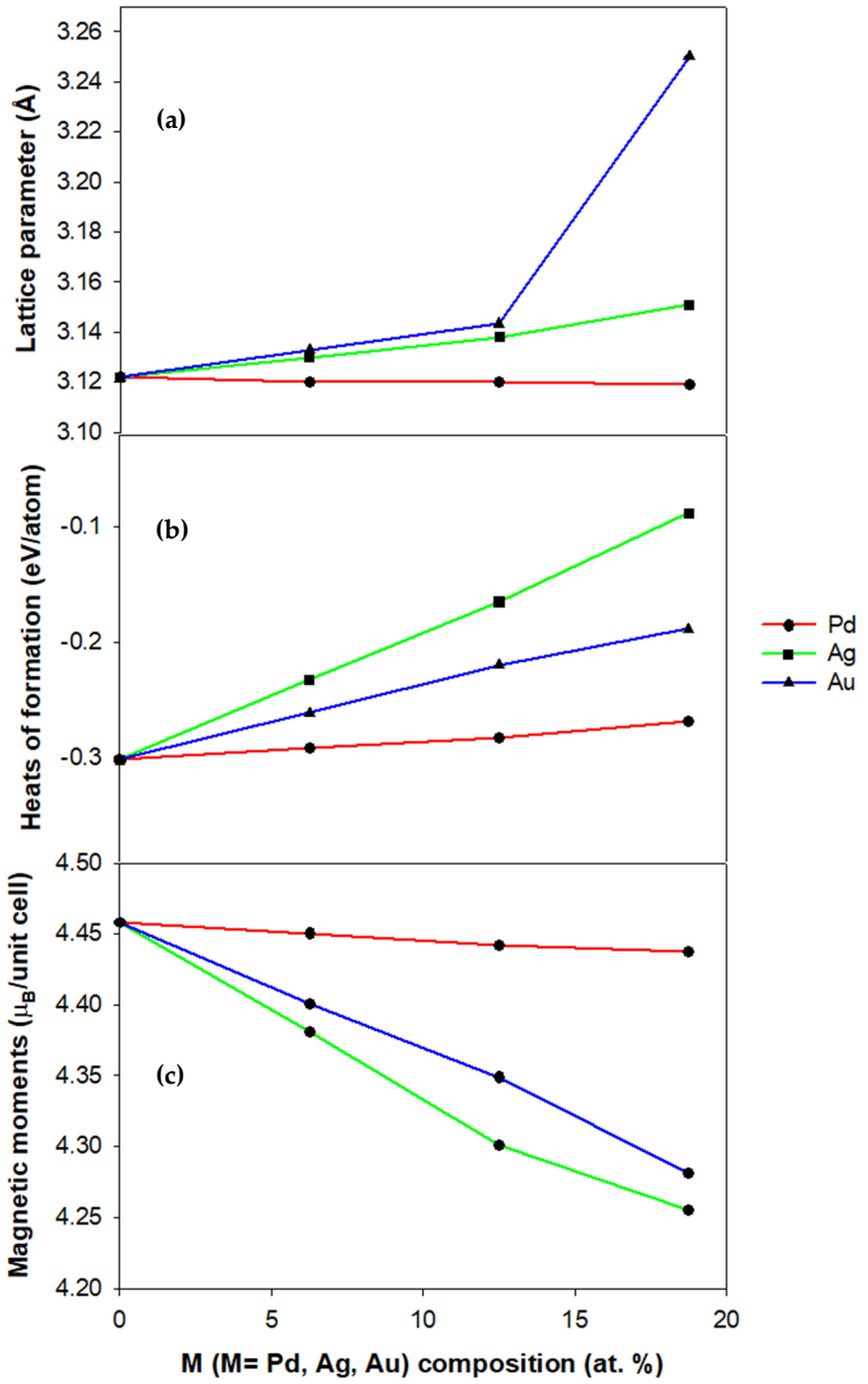

Figure 2. (**a**) Lattice parameters, (**b**) heats of formation and (**c**) magnetic moments against at. % M for B2 FM $Mn_{50}Pt_{50-x}M_x$ alloys (x = 6.25, 12.50 and 18.75).

However, a further increase in Pd content results in a slight gradual reduction in magnetic moment, as shown in Figure 2c. The addition of Pd on B2 FM MnPt alloy resulted in the ferromagnetic behavior being maintained. The magnetic moments decrease with an increase in the composition, suggesting that Ag is not good at enhancing the magnetism of MnPt alloy (see Figure 2c). At 18.75 at. % Ag, the structure has lower magnetism for B2 $Mn_{50}Pt_{50-x}Ag_x$. From the magnetism results, it can be distinguished that the ferromagnetic behavior can be observed below 18.75 at. % Ag and above this, antiferromagnetic/paramagnetic behavior can be activated. It is observed that the magnetic moments reduce when Au is introduced to the MnPt alloy. Generally, this work suggests

that ferromagnetism is observed but reduces with an increase in Au for 6.25, 12.5 and 18.75 at. %. The precious metal with a smaller atomic radius (Pd) showed an improvement as compared to the elements with a bigger atomic radius i.e., Ag and Au. This suggests that elements such as Pd with their smaller atomic radius can enhance the ferromagnetism of MnPt alloy.

The partial magnetic moments of B2 FM $Mn_{50}Pt_{50-x}M_x$ alloys are highlighted in Table 1. This indicates the magnetic contribution of each atom in the total magnetic moments in the compound. It is observed that Mn atoms contribute more to the total magnetic moments of the binary B2 FM MnPt alloys, as explained above with the Pt atom contributing less, suggesting that indeed the structure shows ferromagnetic behavior. As the amount of Pd is added, it is also observed that Mn atoms contribute more while Pt and Pd contribute almost the same but less due to their atomic size. More interestingly, the contribution of Mn atoms increases slightly, while Pt and Pd atoms reduce with an increase in composition as shown in Table 1.

Table 1. The atomic partial magnetic moments (μ_B/unit cell) of B2 FM $Mn_{50}Pt_{50-x}M_x$ alloys (x = 6.25, 12.50, 18.75 and 25), where M = Pd, Ag, and Au.

Composition	Mn	Pt	M
$Mn_{50}Pt_{50}$	3.784	0.667	
	$Mn_{50}Pt_{50-x}Pd_x$		
$Mn_{50}Pt_{43.75}Pd_{6.25}$	3.788	0.407	0.360
$Mn_{50}Pt_{37.5}Pd_{12.5}$	3.792	0.398	0.365
$Mn_{50}Pt_{31.25}Pd_{18.75}$	3.797	0.404	0.356
	$Mn_{50}Pt_{50-x}Ag_x$		
$Mn_{50}Pt_{43.75}Ag_{6.25}$	3.773	0.411	0.062
$Mn_{50}Pt_{37.5}Ag_{12.5}$	3.756	0.374	0.060
$Mn_{50}Pt_{31.25}Ag_{18.75}$	3.758	0.355	0.056
	$Mn_{50}Pt_{50-x}Au_x$		
$Mn_{50}Pt_{43.75}Au_{6.25}$	3.783	0.401	0.114
$Mn_{50}Pt_{37.5}Au_{12.5}$	3.780	0.376	0.112
$Mn_{50}Pt_{31.25}Au_{18.75}$	3.765	0.362	0.096

This suggests that the addition of Pd slightly improves the magnetism of the B2 FM MnPt alloy and that the presence of Mn atoms contributes to the ferromagnetic behavior. This indicates that the directions of electron spins are aligned parallel to each other due to the exchange interaction for all the compositions. In the case of the addition of Ag, it is noted that Mn atoms contribute more to the total magnetic moment as compared to Pt and Au. The contribution decreases with an increase in Ag composition. This suggests that Ag cannot be used to improve the ferromagnetism of B2 FM MnPt alloy as it may transform the system to paramagnetic. When Au is added, the Mn atoms contribute more as compared with the Ag addition. The contribution of Mn atoms decreases with an increase in Au compositions. This suggests that the ferromagnetism is compromised when Mn atoms contribute less. The Au tends to contribute less towards the total magnetic moments. It is noted that the precious elements do not contribute antiferromagnetism on the Pt-site but only ferromagnetism below 18.75 at. % M. The overall observation is that the Pt contribution to the magnetic moment is due to unpaired electrons in the d-orbital, so that when d^{10} is added it reduces the magnetic moment.

3.2. Elastic Properties

The mechanical properties of a solid can be obtained through its elastic constants. These characteristics can be used to characterize a crystal's ability to withstand external stress. Additionally, they offer crucial details regarding bonding properties close to the equilibrium state. Investigating the elastic constants is therefore crucial to comprehending the mechanical behavior of $Mn_{50}Pt_{50-x}M_x$ alloys. Based on energy variation, theoretical elastic constants were computed for the equilibrium lattice configuration under mild

strains. A relaxed unit cell lattice structure is subjected to a suitable set of strains. The resulting change in total energy on the deformation is then used to calculate the elastic constants. They can differ depending on the type of lattice i.e., for the cubic lattice there are three (C_{11}, C_{12}, C_{44}) independent elastic constants [26,27]. The elastic properties revealed diverse elastic behavior of the B2 $Mn_{50}Pt_{50}$ structure. According to [27], the cubic system's mechanical stability condition is as follows:

$$C_{44} > 0;\ C_{11} > C_{12} \text{ and } C_{11}+2C_{12} > 0, \quad (2)$$

For the structure to be stable, the stability criterion for the elastic constants needs to be met. The following tables and figures present the calculated single-crystal elastic constants for these compounds as reported in this paper.

For practical purposes, mechanical properties like bulk modulus (B), shear modulus (G), Young's modulus (E), hardness (Hv), and Poisson's (v) ratio can also be calculated using elastic constants. In this paper, Young's modulus (E) is calculated to estimate the physical stiffness of the $Mn_{50}Pt_{50-x}M_x$ alloys and is presented in the tables below. It is more rigid and less likely to deform if the value of E is higher.

Using the mechanical properties of these compounds, we analyzed their ductility using Poisson's ratio. Metals with a Poisson's ratio $\geq$0.26 are regarded as ductile, whereas metals having a Poisson's ratio less than 0.26 are referred to as being brittle [28]. One crucial property of materials that can be used to gauge its capacity to withstand localized deformation is its hardness (Hv) [29]. To determine the hardness (Hv), the following calculation can be used:

$$H_V = \frac{E(1-2v)}{6(1+v)}, \quad (3)$$

where v stands for Poisson's ratio and E stands for Young's modulus. The following tables display the calculated Hv of $Mn_{50}Pt_{50-x}M_x$.

Table 2 presents the calculated elastic constants of B2 $Mn_{50}Pt_{50}$ phases along with the available theoretical information. In order to describe the mechanical stability of the binary $Mn_{50}Pt_{50}$ alloy, we follow the stability criteria in Equation (2). PM-B2 $Mn_{50}Pt_{50}$ appears to have the highest value of C_{12} which is greater than C_{11}, and thus leading to C′ being negative, an indication of mechanical instability at 0 K. This is in agreement with experimental data suggesting that B2 PM $Mn_{50}Pt_{50}$ is a high-temperature phase. The predicted elastic constants for PM-B2 $Mn_{50}Pt_{50}$ confirm the findings from the theoretical view within 5% [24] as shown in the parenthesis. It is noted that FM-B2 $Mn_{50}Pt_{50}$ satisfies all the cubic mechanical stability criteria as stipulated in Equation (2).

Table 2. Elastic constants of PM and FM MnPt structures at 50 at. % Pt. The theoretical values are given in parentheses.

Elastic Constants, C_{ij} (GPa)	PM-B2 $Mn_{50}Pt_{50}$	PM-B2 $Mn_{50}Pt_{50}$
C_{11}	68 (68)	201
C_{12}	330 (329)	154
C_{44}	138 (134)	101
C′	−131 (−131)	23

3.2.1. $Mn_{50}Pt_{50-x}Pd_x$

Figure 3 displays the computed elastic constants for the B2 $Mn_{50}Pt_{50-x}Pd_x$ alloys ($0 \leq x \leq 18.75$). For the structure to be stable, the stability criterion for the elastic constants needs to be met. Figure 3 illustrates that none of the predicted Cijs for B2 $Mn_{50}Pt_{50-x}Pd_x$ satisfy the stability criteria due to C_{11} being less than C_{12}, which produced a negative elastic shear modulus ($C' < 0$). A negative C′ on Pd addition signals a possible martensitic transformation (MT).

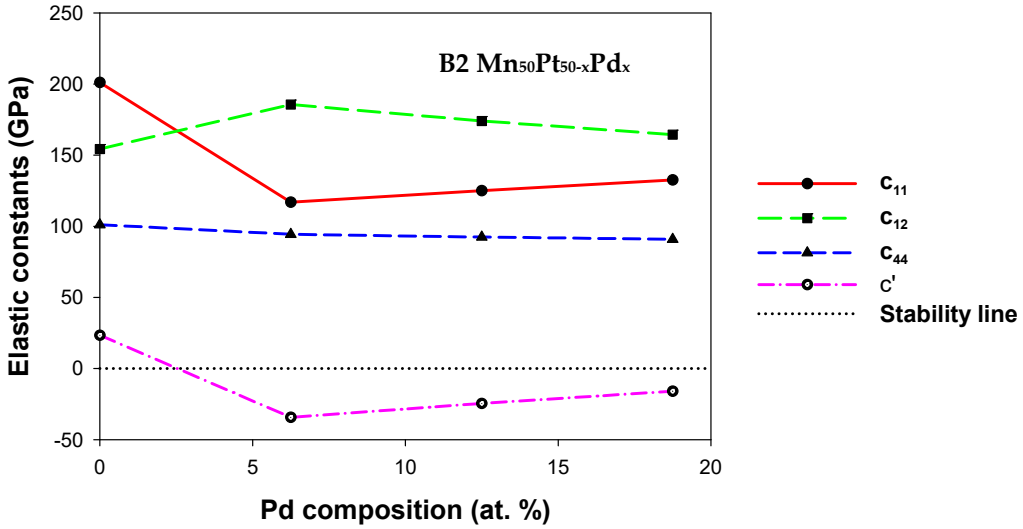

Figure 3. Elastic constants (GPa) of B2 $Mn_{50}Pt_{50-x}Pd_x$ ($0 \leq x \leq 18.75$) ternary alloys.

In order to determine the stiffness of the B2 $Mn_{50}Pt_{50-x}Pd_x$, we calculated Young's modulus, as shown in Table 3. It is observed that the B2 $Mn_{50}Pt_{50-x}Pd_x$ alloy has lower Young's modulus value, indicating the least stiffness and the ability to deform conveniently. The findings imply that the addition of Pd does not improve the $Mn_{50}Pt_{50}$ alloy's stiffest point.

Table 3. The calculated Young's modulus E (GPa), Poisson's ratio (v), and hardness (Hv) (GPa) of $Mn_{50}Pt_{50-x}Pd_x$ alloy.

Structure	Young's Modulus (GPa)	Poisson's Ratio	Hardness (GPa)
$Mn_{50}Pt_{50}$	184.69	0.32	6.80
$Mn_{50}Pt_{43.75}Pd_{6.25}$	118.38	0.38	2.90
$Mn_{50}Pt_{37.5}Pd_{12.5}$	124.90	0.37	3.36
$Mn_{50}Pt_{31.25}Pd_{18.75}$	128.51	0.36	3.66

Poisson's ratio (v) was used to analyze the ductility of B2 $Mn_{50}Pt_{50-x}Pd_x$ alloys as indicated above. The v was greater than 0.26 for B2 $Mn_{50}Pt_{50-x}Pd_x$ alloys, which implies that the structures have ductile behavior. The results suggest that B2 $Mn_{50}Pt_{43.75}Pd_{6.25}$ is more ductile with the highest values of v. For B2 $Mn_{50}Pt_{50-x}Pd_x$ alloys, it is observed that the Hv decreases as Pd increases ($0 \leq x \leq 18.75$). It appears from the findings that adding Pd will not yield the hardest material.

3.2.2. $Mn_{50}Pt_{50-x}Ag_x$

The elastic constants of the structures for B2 $Mn_{50}Pt_{50-x}Ag_x$ ($0 \leq x \leq 18.75$) with the addition of Ag are displayed in Figure 4. The elastic constants C_{11}, C_{12} and C_{44} are positive for B2 $Mn_{50}Pt_{50-x}Ag_x$, as shown in Figure 4. However, C_{11} decreases with the addition of Ag content while C_{12} increases, suggesting that the structure is becoming mechanically unstable (breaking stability condition, $C_{11} > C_{12}$). This is evident at 6.25 and 12.50 at. % Ag, where C′ is negative, thus rendering the structures mechanically unstable at these concentrations. On the contrary, a slight mechanical stability is observed at 18.75 at. % Ag. The results for 6.25 and 12.50 at. % Ag suggest a possible (MT) due to negative C′ in this composition range.

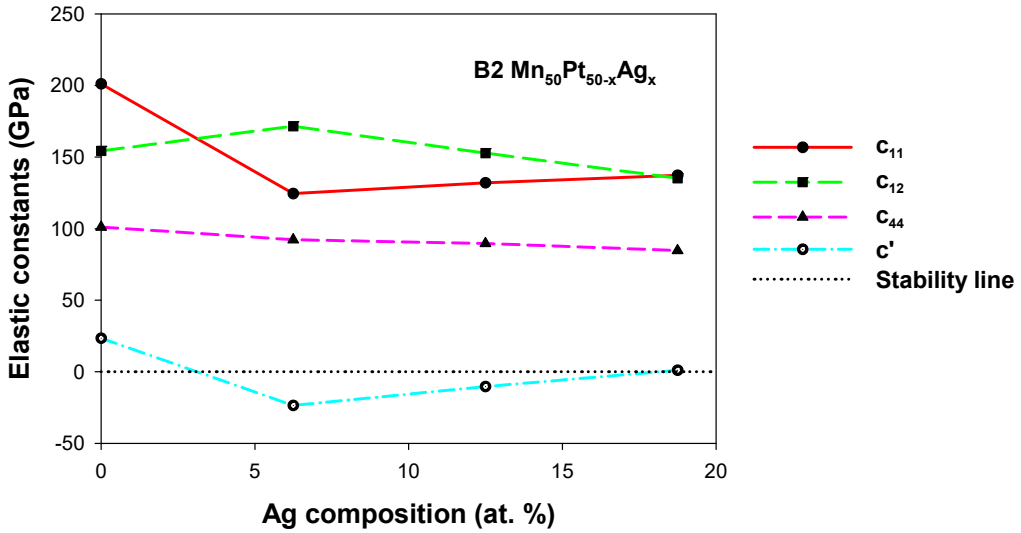

Figure 4. Elastic constants (GPa) of the B2 $Mn_{50}Pt_{50-x}Ag_x$ ($0 \leq x \leq 18.75$) ternary alloys.

The predicted Young's (E) modulus, hardness (Hv) and Poisson's ratio (v) are shown in Table 4. It can be seen that the E values reduce with an increase in Ag composition for B2 $Mn_{50}Pt_{50-x}Ag_x$ alloys, which means that the structures have less ability to resist elastic deformations.

Table 4. The calculated Young's modulus E (GPa), Poisson's ratio (v), and hardness (H) (GPa) of $Mn_{50}Pt_{50-x}Ag_x$ alloy.

Structure	Young's (Gpa)	Poisson Ratio	Hardness (Gpa)
$Mn_{50}Pt_{50}$	184.69	0.32	6.80
$Mn_{50}Pt_{43.75}Ag_{6.25}$	125.43	0.37	3.44
$Mn_{50}Pt_{37.5}Ag_{12.5}$	133.67	0.35	4.28
$Mn_{50}Pt_{31.25}Ag_{18.75}$	133.24	0.34	4.66

The ductility and brittleness of the B2 $Mn_{50}Pt_{50-x}Ag_x$ alloys were estimated using Poisson's ratio (v). The results showed that the binary B2 phase does satisfy the stability criteria, as v is greater than 0.26. When Ag was introduced, the v values were found to be greater than 0.26, which suggests that the structures are ductile.

As shown in Table 4, the values of hardness decrease with an increase in Ag concentration. The addition of Ag was found not to be the best choice to improve the hardness of the $Mn_{50}Pt_{50}$ alloy.

3.2.3. $Mn_{50}Pt_{50-x}Au_x$

The computed elastic constants for $Mn_{50}Pt_{50-x}Au_x$ alloys ($0 \leq x \leq 18.75$) are displayed in Figure 5. It is observed that for the intended compositions of B2 $Mn_{50}Pt_{50-x}Au_x$ alloys ($0 \leq x \leq 18.75$), all independent elastic constants C_{11}, C_{12}, and C_{44} are positive. At small Au content (6.25 and 12.50 at. %), the C′ is negative, indicating a potential MT since it makes the structures mechanically unstable at those concentrations. It is noteworthy that above 18.75 at, the elastic shear modulus (C′) exhibits positivity, which indicates that the structures are mechanically stable at high Au content. The results suggest that the Au composition above 18.75 at.% may hinder further transformation to low-temperature phase.

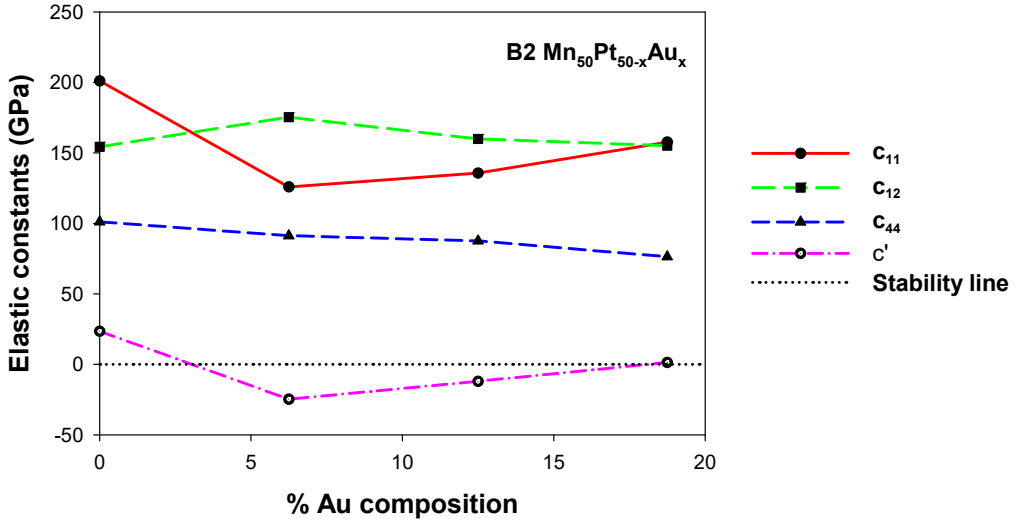

Figure 5. Elastic constants (GPa) of the B2 $Mn_{50}Pt_{50-x}Au_x$ ($0 \leq x \leq 18.75$) ternary alloys.

Table 5 shows the calculated Young's (E) modulus, hardness (Hv) and Poisson's (v) ratios for B2 $Mn_{50}Pt_{50-x}Au_x$ alloys ($0 \leq x \leq 18.75$). As composition increases, the E values are observed to decrease, indicating that Au has the lowest resistance to elastic deformations. The calculated v is greater than 0.26 for B2 $Mn_{50}Pt_{50-x}Au_x$ alloys ($0 \leq x \leq 18.75$) which suggests that the structures are ductile. Furthermore, it is noted that hardness decreases with an increase in Au concentration as shown in Table 5. Due to the small values of Hv, the predicted results showed that Au addition does not have the strongest ability to enhance the hardness of the binary $Mn_{50}Pt_{50}$ system.

Table 5. The calculated Young's modulus E (GPa), Poisson's ratio (σ), and hardness (Hv) (GPa) of $Mn_{50}Pt_{50-x}Au_x$ alloy.

Structure	Young's Modulus (GPa)	Poisson's Ratio	Hardness (GPa)
$Mn_{50}Pt_{50}$	184.69	0.32	6.80
$Mn_{50}Pt_{43.75}Au_{6.25}$	123.00	0.37	3.23
$Mn_{50}Pt_{37.5}Au_{12.5}$	129.53	0.36	3.81
$Mn_{50}Pt_{31.25}Au_{18.75}$	150.42	0.33	5.53

3.3. Vibrational Properties of PM and FM B2 MnPt Structures at 50 at. % Pt

Figure 6 displays the computed phonon dispersion curves for the PM and FM MnPt structures. The dispersion curves show two different kinds of phonons: the acoustic and optical modes, which correspond to the lower and upper sets of curves in the diagram, respectively. Since there are soft modes seen, our phonon dispersion calculations confirm that the PM B2 MnPt structure is unstable, as seen in elastic constants (Table 2). The soft modes are observed along the R, X, and M directions. The pure elastic instability $C' = ½ (C_{11} - C_{12}) < 0$ is represented by the downward slope of the acoustic Γ-M branch. These soft modes suggest that the structure is vibrationally unstable with the potential to undergo a phase transition to lower-temperature phases. Furthermore, the FM MnPt structure displays no soft modes (positive frequency) in the phonon dispersion curve which corresponds to the most stable structure behavior as predicted by the elastic constants. This implies that there is no phase transition of the structure to lower temperature phases like $L1_0$.

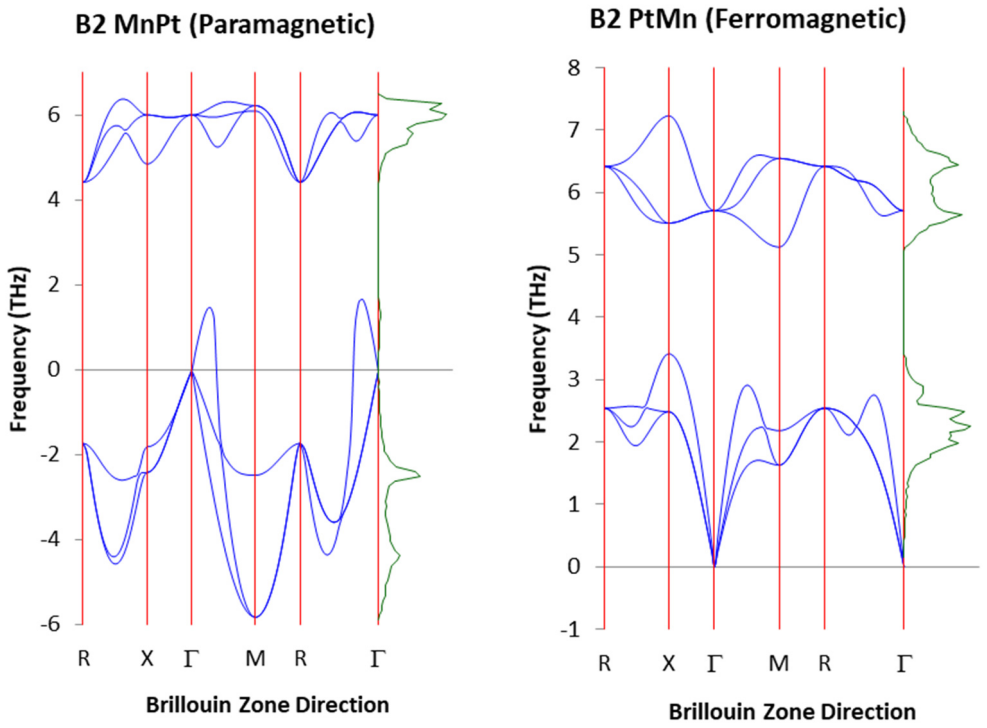

(**a**) (**b**)

Figure 6. Phonon dispersion curves for (**a**) PM and (**b**) FM B2 MnPt alloy.

4. Conclusions

The lattice parameters, heats of formation, magnetic moments, and mechanical properties of $Mn_{50}Pt_{50-x}M_x$ (M = Pd, Ag, Au) alloys ($0 \leq x \leq 18.75$) were successfully studied for possible spintronic applications using the ab initio DFT approach. The available experimental and theoretical values of lattice parameters showed good agreement with our results, within 5%. Based on calculated heats of formation, current results suggest that thermodynamic stability can be maintained for B2 $Mn_{50}Pt_{50-x}Pd_x$ alloys ($0 \leq x \leq 18.75$) while it is significantly reduced by the addition of Au and Ag. It was revealed that ferromagnetism is maintained with Pd addition but significantly reduced in the case of Au and Ag. The elasticity results of B2 $Mn_{50}Pt_{50-x}Ag_x$ and $Mn_{50}Pt_{50-x}Au_x$ at compositions between 6.25 and 12.50 signal a possible martensitic transformation to a lower symmetry phase due to $C' < 0$ but regain mechanical stability at 18.75 at%. On the contrary, the mechanical stability criteria are never satisfied in B2 $Mn_{50}Pt_{50-x}Pd_x$. It was further revealed using the values of the Poisson's ratio that an increase in Pd, Ag, and Au could effectively improve the ductility of the B2 $Mn_{50}Pt_{50-x}M_x$ compounds.

Pd, Ag, and Au could effectively improve the ductility of the compound.

Author Contributions: Conceptualization, R.D. and M.P.; methodology, H.C.; software, P.N.; validation, M.P.; formal analysis, R.D.; investigation, M.P.; resources, P.N.; data curation, M.P.; writing—original draft preparation, R.D.; writing—review and editing, R.D. and M.P.; visualization, R.D.; supervision, M.P.; project administration, J.M.; funding acquisition, J.M. All authors have read and agreed to the published version of the manuscript.

Funding: This research received no external funding.

Institutional Review Board Statement: Not applicable.

Informed Consent Statement: Not applicable.

Data Availability Statement: Data are contained within the article.

Acknowledgments: The Materials Modelling Centre, University of Limpopo, provided computational resources for the work, which was completed at Mintek. It is our pleasure to acknowledge the outstanding computing resources provided by the Cape Town High-Performance Computing Center (CHPC). The Department of Science and Innovation (DSI)'s Advanced Materials Initiative (AMI) through Mintek provided financial support, which the authors acknowledge. The Department of Science and Innovation's South African Research Chair Initiative is greatly appreciated for its support.

Conflicts of Interest: The authors declare no conflict of interest.

References

1. Coey, J.M.D. Permanent magnets: Plugging the gap. *Scr. Mater.* **2012**, *67*, 524–529. [CrossRef]
2. Umetsu, R.Y.; Sakuma, A.; Fukamichi, K. Magnetic anisotropy energy of antiferromagnetic $L1_0$-type equiatomic Mn alloys. *Appl. Phys. Lett.* **2006**, *89*, 052504. [CrossRef]
3. Sakuma, A.; Umetsu, R.Y.; Fukamichi, K. Magnetic structures and their stability in Mn3Rh ordered and disordered alloys. *Phys. Rev. B* **2002**, *66*, 014432. [CrossRef]
4. Park, I.J.; Lee, T.; Das, P.; Debnath, B.; Carman, G.P.; Lake, R.K. Strain control of the Néel vector in Mn-based antiferromagnets. *Appl. Phys. Lett.* **2019**, *114*, 142403. [CrossRef]
5. Jenkins, S.; Chantrell, R.W.; Evans, R.F.L. Atomistic simulations of the magnetic properties of Ir_xMn_{1-x} alloys. *Phys. Rev. Mater.* **2021**, *5*, 034406. [CrossRef]
6. Tsang, C.; Chen, M.M.; Yogi, T. Gigabit-density magnetic recording. *Proc. IEEE* **1993**, *81*, 1344. [CrossRef]
7. Puebla, J.; Kim, J.; Kondou, K.; Otani, Y. Spintronic devices for energy-efficient data storage and energy harvesting. *Commun. Mater.* **2020**, *1*, 1–9. [CrossRef]
8. Farrow, R.F.C.; Marks, R.F.; Gider, S.; Marley, A.C.; Parkin, S.S.P.; Mauri, D. Mn_xPt_{1-x}: A new exchange bias material for Permalloy. *J. Appl. Phys.* **1997**, *81*, 4986. [CrossRef]
9. Lin, T.; Gorman, G.L.; Tsang, C. Antiferromagnetic and hard-magnetic stabilization schemes for magneto-resistive sensors. *IEEE Trans. Magn.* **1996**, *32*, 3443.
10. Kishi, H.; Kitade, Y.; Miyake, Y.; Tanaka, A.; Kobayashi, K. Study of exchange-coupled bias field in Ni-Fe/Pd-Pt-Mn thin films. *IEEE Trans. Magn.* **1996**, *32*, 3380. [CrossRef]
11. Lu, Z.; Chepulskii, R.V.; Butler, W.H. First-principles study of magnetic properties of L10-ordered MnPt and FePt alloys. *Phys. Rev. B* **2012**, *81*, 094437. [CrossRef]
12. Umetsu, R.Y.; Fukamichi, K.; Sakuma, A. Electrical and Magnetic Properties, and Electronic Structures of Pseudo-Gap-Type Antiferromagnetic L10-Type MnPt Alloys. *Mater. Trans.* **2006**, *47*, 2–10. [CrossRef]
13. Krén, E.; Kádár, G.; Pál, L.; Sólyom, J.; Szabó, P.; Tarnóczi, T. Magnetic Structures and Exchange Interactions in the Mn-Pt System. *Phys. Rev.* **1968**, *171*, 574. [CrossRef]
14. Ladwig, P.F.; Chang, Y.A. Paramagnetic to antiferromagnetic phase transformation in sputter deposited Pt–Mn thin films. *J. Appl. Phys.* **2003**, *94*, 979–987. [CrossRef]
15. Alsaad, A.; Ahmad, A.A.; Obeidat, T.S. Structural, electronic and magnetic properties of the ordered binary FePt, MnPt, and CrPt3 alloys. *Heliyon* **2020**, *6*, e03545. [CrossRef]
16. Diale, R.; Ngoepe, P.; Moema, J.; Phasha, M.; Chauke, H. Thermodynamic and magnetic properties of Pt50Mn50-xMx (M = Cr, Fe) alloys: A first-principles study. *MATEC Web of Conf.* **2022**, *370*, 02006. [CrossRef]
17. Diale, R.G.; Ngoepe, P.E.; Moema, J.S.; Phasha, M.J.; Moller, H.; Chauke, H.R. A computational study of the thermodynamic and magnetic properties of Co-alloyed MnPt. *MRS Adv.* **2023**, *8*, 651–655. [CrossRef]
18. Kresse, G.; Hafner, J. Ab initio molecular dynamics for liquid metals. *Phys. Rev. B* **1993**, *47*, 58–561. [CrossRef]
19. Kresse, G.; Furthmüller, J. Efficient iterative schemes for ab initio total-energy calculations using a plane-wave basis set. *Phys. Rev. B* **1996**, *54*, 11169–11186. [CrossRef]
20. Kohn, W.; Sham, L.J. Self-Consistent Equations Including Exchange and Correlation Effects. *Phys. Rev.* **1965**, *140*, 1133–1138. [CrossRef]
21. Perdew, J.P.; Burke, K.; Ernzerhof, M. Generalized Gradient Approximation Made Simple. *Phys. Rev. Lett.* **1996**, *77*, 3865. [CrossRef] [PubMed]
22. Monkhorst, H.J.; Pack, J.D. Special points for Brillouin-zone integrations. *Phys. Rev. B* **1996**, *13*, 5188–5192. [CrossRef]
23. Voigt, W. Textbook of crystal physics. *Ann. Phys. Chem.* **1889**, *274*, 573–586. [CrossRef]
24. Parlinski, K.; Li, Z.Q.; Kawazoe, Y. First-Principles Determination of the Soft Mode in Cubic ZrO. *Phys. Rev. Lett.* **1997**, *78*, 4063–4066. [CrossRef]
25. Wang, J.; Gao, A.; Chen, W.; Zhang, X.D.; Zhou, B.; Jiang, Z. The structural, elastic, phonon, thermal and electronic properties of MnX (X=Ni, Pd and Pt) alloys: First-principles calculations. *J. Magn. Magn. Mater.* **2013**, *333*, 93–99. [CrossRef]
26. Mahlangu, R.; Phasha, M.J.; Chauke, H.R.; Ngoepe, P.E. Structural, elastic and electronic properties of equiatomic PtTi as potential high temperature shape memory Alloy. *Intermetallics* **2013**, *3*, 27–32. [CrossRef]

27. Mehl, M.J.; Klein, B.M. First-principles calculation of elastic properties. In: Westbrook JH, Fleischer RL, editors. Intermetallic Compounds–Principles and Practice. Vol. 1. London: John Wiley and Sons, Ltd. *Intermet. Compd.* **1994**, *1*, 195–210.
28. Frantsevich, I.N.; Voronov, S.A. *Handbook on Elastic Constants and Moduli of Elasticity for Metals and Nonmetals*; Naukova Dumka: Kiev, Ukraine, 1983; pp. 60–180.
29. Yi, G.; Zhang, X.; Qin, J.; Ning, J.; Zhang, S.; Ma, M.; Liu, R. Mechanical, electronic and thermal properties of Cu_5Zr and Cu_5Hf by first-principles calculations. *J. Alloys Compd.* **2015**, *640*, 455–461. [CrossRef]